An Environmentally Friendly Nanocomposite Polypyrrole@Silver/Reduced Graphene Oxide With High Catalytic Activity for Bacteria and Antibiotics

Chun Liu
Jiangsu University of Science and Technology
Fangyan Chen (chenfangyan@just.edu.cn)
Jiangsu University of Science and Technology https://orcid.org/0000-0002-7496-7797
Yu-bin Tang
Jiangsu University of Science and Technology
Peng-wei Huo
Jiangsu University

Research Article

Keywords: Nano silver, Polypyrrole, Antibacterial activity, Photocatalytic activity

Posted Date: March 5th, 2021

DOI: https://doi.org/10.21203/rs.3.rs-274353/v1

Abstract

In this study, PPy@Ag/rGO nanocomposites were successfully synthesized via the one-pot hydrothermal mothed using graphene oxide, pyrrole monomer and silver nitrate. The structures and morphologies of as-obtained PPy@Ag/rGO ternary nanocomposites were systematically investigated by scanning electron microscopy (SEM) and transmission electron microscope (TEM). It was found that the PPy@Ag NPs were well-distributed on the reduction graphene oxide nanoflakes. The minimum inhibitory concentration (MIC) demonstrated that the PPy@Ag/rGO had enhanced antimicrobial efficiency with Gram-negative (*Escherichia coli*) bacteria compared with that at the same concentration of silver. From liquid antibacterial cycle experiments, the addition of polypyrrole contributes to the stability of nanosilver and reducing the loss of nanosilver. After several cycles, the antibacterial rate of PPy@Ag/rGO nanomaterials can still be maintained above 90%. In addition, the photocatalytic degradation of tetracycline (TC) under visible light displayed that the composite had good photocatalytic activity and catalytic stability.

1. Introduction

Nano silver and silver compounds have potential antibacterial activity against a far-ranging of microorganisms. And these antibacterial materials have been widely used in many sterilization applications [1, 2]. Nano sliver is an intolerant disinfectant, which can significantly reduce the use of many bacterial infections, such as benzyl penicillin and tetra, as compared with the general presence. Some bacteria in the environment are resistant to antibiotics, such as *Staphylococcus aureus* (*S.aureus*) and *Escherichia coli* (*E.coli*) are resistant to penicillin benzyl. Therefore, Ag NPs have attracted much attention when nano-silver is found to be effective in killing a many kind of viruses, eumycetes and bacteria. The principium of Ag NPs on bacteria sterilization is not completely clarity. It has been suggested that the antibacterial activity is founded on the electrostatic force between the negatively charged pericellular membrane of the germ and the positively charged Ag ions. As a result, Ag ions can lead to bacterial death by destroying the pericellular membrane, intensely interacting with the sulfhydryl radicals of active enzymes, and even damaging DNA replication capabilities [3, 4]. Precious metal plasmas has a localized surface plasmon effect. The surface can generate high-energy hot electrons, and high-energy hot electrons can participate in the reaction [5, 6]. This phenomenon will help to improve the photocatalytic ability [7, 8]. This will effectively reduce the emergence of super bacteria in the environment. It was apparent to all that the antibacterial activity of silver nanoparticles is closely connected to their particle size and spatial distribution [9]. The smaller the particle size of nano-silve is, the better the antibacterial effect is. However, small size silver nanoparticles tend to gather in the preparation process to minimize the surface energy, which results in a significant abasement of their antibacterial performance.To overcome this disadvantage, it is important to discover and find a suitable carrier material to effectively disperse silver nanoparticles [10, 11]. Ali et al. and Tripathi et al. have reported the Ag-doped TiO_2 nanocomposites showed high catalytic activity under visible light and strong inhibition of various bacterial strains [12]. Liu et al. [13] have reported that Ag/ZnO composites have

enhanced photocatalytic activity for organic contaminants driven by visible light and synergistically enhanced antibacterial activity against gram bacteria.

Reduced graphene oxide (rGO) is acknowledged as a single layer of carbon atoms that forms a serried honeycomb structure with oxhydryl and epoxy functional groups on two approachable sides and carboxyl groups on the brinks [14–16]. These functional groups can better support other materials such as nanometals on the surface of rGO. In 2010, the research first reported the antibacterial activity of graphene oxide (GO) and rGO, where graphene-based nanomaterials have been shown to be effective in choking back the propagation of *E.coli* [17]. For example, many studies of graphene-based materials have shown that the physical interaction between bacterial pericellular membrane and rGO. The sharp edges of reduced graphene oxide can destroy bacterial membrane fracture by puncturing [18]. This local disturbance affects the film potential of phospholipid bilayer of bacterial membrane, interferes with cell metabolic process, and ultimately destroys the pericellular membrane, leading to the cracking and death of bacterial cells [19]. The oxidative stress cause by rGO nanoparticles may particapate in irreparable impairment to the bacterial cells that lead to the destruction of cell completeness [20, 21].The damage of graphene to pericellular membrane may also be due to the electric-charge transfer mutual effect cause by direct contact between microbiological membranes and graphene [22]. In addition, rGO has inimitable characteristics, including comparatively large specific surface area, lower cytotoxicity and favourable water stability [23, 24]. Therefore, it can be used as a plain stage for growth of metal nanoparticles. This form of composite material has been widely used in the field of photocatalysis. The carboxyl group on surface of rGO base allows Ag NPs to interact with rGO nanoparticles through physical adsorption. Specially, the silver positively charged ion can be straightway connected to the carboxy group on the superficies of rGO through electrostatic interactions. Therefore, deoxidization occurs on superficies of GO nano-films, forming a steady rGO-Ag nano-complex. By adding rGO as the carrier, Ag NPs aggregation problems can be minimized or even prevented. Huo et al. [25] have reported Ag/Ag_2S/rGO displayed enhanced photocatalytic and antibacterial activity.

However, the Ag nanoparticles supported on the surface of the reduced graphene oxide are easily peeled off during use. So how to avoid the loss of nano silver during use is an urgent problem to be solved. In the past decade, antimicrobial conductive polymerized substance show well foreground for development due to their favorable biocompatibility and chemical stability,non-volatility, lack of spread on the skin, low poisonous character, biological activity and long retention time [26–28]. Polypyrrole (PPy) is shaped from plenty of linked pyrrole ring architectures and is one of the representative antimicrobial polymerized substances. And PPy has been displayed to possess well antibacterial activity against *E.coli* [29]. The antibacterial principium of polypyrrole is probably ascribed to seepage of cytoplasm since the mutual effect of bacteria cell membrane and the positive electrical charges in PPy chains. In addition, polypyrrole (PPy) is an organic semiconductor with a narrow band gap, strong electron transport capability and redox properties [30–33]. Therefore, PPy is widely used in the field of photocatalysis. Polypyrrole is usually prepared by oxidation of pyrrole by chemical or electrochemical means [34–36]. Wan et al. and Li et al. have reported the inosculation of cellulose hydrogel and Ag nanoparticles to PPy contribute to the

stabilization of the nanomaterial [37]. The addition of polypyrrole can improve the disadvantage of poor stability of binary Ag/rGO nano-composite during antimicrobial activity. Therefore, it is of great significance to design a simple system to develop nano-composites with excellent antibacterial properties.

In this work, the PPy@Ag/rGO nano antibacterial material was synthesized by hydrothermal method. The photocatalytic activities of PPy@Ag/rGO were researched by degrading TC under visible light irradiation. The PPy@Ag/rGO nanomaterial prepared by our research institute was used as an antibacterial agent to inactivate *E.coli* for 12 h at 37°C. At the same time, we further studied the antibacterial effect of PPy on the liquid antibacterial cycle experiment.

2. Experimental Section

2.1 Materials

Silver nitrate ($AgNO_3$), ferric chloride ($FeCl_3$), polyvinylpyrrolidone (PVP) and Ethylene glycol ($(CH_2OH)_2$), were purchased from Sinopharm Chemical Reagent Co., Ltd. (Shanghai, China). Pyrrole was purchased from Shanghai Aladdin Biochemical Technology Co., Ltd. All of the chemical reagents used in the experiments were analytical reagents and did not require further purification. The deionized water used in this experiment also did not require any purification treatment.

2.2 Synthesis of PPy@Ag/rGO nanocomposite

GO was prepared by the modified Hummers method [38]. The pyrrole monomer was stored in a freezer and distilled under high-purity N_2 prior to use. A 1.5 g polyvinylpyrrolidone (PVP) was added into 75 mL ethylene glycol (EG) to stir well, and then 0.05 g $AgNO_3$ was added to the above solution. The above mixed solution was thoroughly stirred at room temperature for 24 h to prepare a silver colloid. Then 35 μL pyrrole monomer (Py) and 0.082 g $FeCl_3$ were sequentially added and continuously stirred at room temperature for 24 h to obtain PPy@Ag. In this experiment, 0.2 g GO was sonicated in ethylene glycol (20 mL) for 100 minutes to obtain a peeled GO suspension. Afterwards, 20 mL GO suspension was added dropwise to the above reaction system and the solution was continuously stirred for 24 h. Lastly, the obtained solution was moved to a 50 mL Teflon lined stainless steel autoclave and then warmed to 200°C in an oven for 24 h. The obtained PPy@Ag/rGO nano antibacterial material was separated through centrifugationby being washed alternately three times with absolute ethanol and deionized water, respectively. The resulting sample was dried in a vacuum oven at 60°C for 12 hours.

2.3 Characterization

Field emission scanning electron microscope (FESEM, JSM 7800F) and transmission electron microscope (TEM, JEM-2100) were used to observe the morphologies. The composition and crystal state of the crystals were determined using an X-ray Diffractometer (XRD-6100Lab, Japan), used Cu-Kα, define a scanning speed of 5°/min, and scanning angles ranging from 5° to 80°. The Fourier transform infrared

(FTIR) spectra were recorded in transmission mode from 4000 cm^{-1} to 500 cm^{-1} on a FTIR spectrometer (Nicolet iS50). The X-ray photoelectron spectroscopy (XPS) measurements were performed on an X-ray photoelectron spectrometer system (Escalab 250Xi) with Al Kα radiation as the excitation source. The binding energies were calibrated by referencing the C 1s peak (284.8 eV) to reduce the sample charge effect. In order to study the active substances such as superoxide radicals ($\bullet O_2^-$) and hydroxyl radicals (•OH) which may be generated in the catalytic process, electron spin resonance (ESR, Bruker A300) spectroscopy was introduced for analysis and the radical scavenger was 5, 5-dimethyl-1-Pyrroline N-oxide (DMPO). The electrochemical impedance (EIS) and transient photocurrent response tests were performed on a CHI 760E electrochemical workstation with 0.5 mol/L Na_2SO_4 solution as the electrolyte. The concentration of silver ions immersed in LB medium was detected by inductively coupled plasma (VISTA-MPX, Australia).

2.4 Antibacterial Tests with PPy@Ag/rGO nanocomposite

The antibacterial activity of composite materials was researched using Gram-negative bacteria *Escherichia coli* (*E. coli*) as a model. Before each antibacterial experiment, all glassware and culture medium must be sterilized in a sterilizer at a temperature of 120°C for 20 minutes. The bacterial strain was cultured on LB liquid culture medium at 37°C for 24 hours to obtain a *E. coli* bacterial suspension. The 30 mg samples were mixed with 200 mL LB liquid culture medium. Afterward, the mixed solution was made the nutrient agar plate in the condition of adding agar powder. Then, the *E. coli* bacterial suspension was diluted by a factor of 10^4, and 30 μL of the solution was evenly spread on a nutrient agar plate. The uniformly coated plates were put in an incubator at 37°C for 24 hours [39]. The damaged *E. coli* and mapping was characterized by using a JSM-7001F FE-SEM operating at 15 kV. To study morphological change of the bacteria cell after contact with nano antibacterial material, bacteria were fixed by using 2.5% paraformaldehyde solution for 1 h, dehydration by using different concentration of ethanol (e.g., 30, 50, 60, 70, 80, 90, and 100% ethanol solutions, each for 2 min). Afterward, the dehydrated bacteria suspension was dropped onto a silicon wafer and allowed to air dry. After spraying gold, it was observed by SEM at an accelerating voltage of 15 kV. At the same time, the dehydrated bacteria suspension was dropped onto a 200-mesh copper mesh and allowed to air dry, and then observed by TEM. The LB liquid culture medium and the *E. coli* suspension were placed in a refrigerator and stored at 4°C. Then, 200 μl of the *E. coli* suspension was put in 50 mL LB liquid culture medium, and 3 mg of the antibacterial material was scattered into the above solution. Afterwards, it was swayed at 37°C for 12 h. The detection limit for this method of quantification is 10 cfu/mL as follows [40]:

Antibacterial rate = $(A_0 - A_t)/A_0 \times 100\%$ (1)

When the A_0 is the cfu of control, A_t the cfu of experimental groups.

2.5 Photocatalytic activity evaluation

Under the irradiation of visible light, the broad-spectrum antibiotic tetracycline (TC) was selected as a photodegradable substance to test the photocatalytic activity of the nanocomposite. The 50 mg of the

catalyst was added to 100 ml 20 mg/L tetracycline solution. The dynamic adsorption equilibrium was achieved by vigorous stirring for 30 min in the absence of light. Then, it was irradiated with a 250 W Xe lamp used as a visible light source for 2 hours, during which time it was sampled every 20 minutes. The absorbance of TC was measured at a wavelength of 357 nm using a UV-vis spectrophotometer.

3. Results And Discussion

3.1 XRD analysis

Figure 1 shows that GO has a sharper peak at 2θ = 11.2˚, which is related to the graphene oxide (001) diffraction layer. Hydroxyl, epoxy, carbonyl and carboxyl functional groups are introduced on the base and edges of the graphite sheet during the deep oxidation of graphite. Therefore, the interlayer spacing (layer spacing: 0.79 nm) of graphene oxide increases and is much higher than that of graphite (layer spacing: 0.34 nm) [41, 42]. The angles of diffraction peaks of Ag/rGO and PPy@Ag/rGO nanocomposites are at 2θ = 37.9˚, 44.1˚, 64.3˚ and 77.3˚ assigned to Bragg's reflections from the (111), (200), (220) and (311) planes of nano silver, which is in agreement (JCPDS No. 00-001-1164) [44]. The diffraction peaks of GO in the nanocomposites PPy@Ag/rGO and Ag/rGO are weakened or almost disappeared, owing to the GO layer is ultrasonically stripped and hydrothermally reduced [43]. It proves that the PPy@Ag/rGO, PPy/rGO and Ag/rGO nanocomposites have been successfully prepared.

3.2 FT-IR spectrum

Figure 2 shows the FT-IR spectrum of PPy@Ag/rGO nanocomposites. The peaks appearing at 1037 cm^{-1} and 1091 cm^{-1} can be attributed to C – C and C – H out of plane deformation stretching and in-plane vibration. The bands at 1187 cm^{-1} and 1474 cm^{-1} are related to stretching of C – N. The band at 1553 cm^{-1} corresponds to C = C stretching of pyrrole ring. The peak appearing at 1712 cm^{-1} is ascribed to C = O stretching of the overoxidation of PPy [44]. The PPy/rGO nanocomposite shows similar peaks as PPy@Ag nanocomposite to some extent. The changes in peak width and displacement of the bands appearing at 668 cm^{-1} and 1037 cm^{-1} are related to the doping state of PPy. This indicates that the PPy@Ag/rGO nanocomposite is successfully synthesized.

3.3 Morphology analysis

The morphologies of the Ag/rGO, PPy/rGO and PPy@Ag/rGO nanocomposite are studied by FESEM (Field emission scanning electron microscopy) analysis (Fig. 3). Figure 3a shows the FESEM image of PPy/rGO nanocomposite obtained from the proposed hydrothermal method. Both graphene oxide and polypyrrole are in the form of flakes and are linked to each other. The agglomeration phenomenon occurs in the nano silver spheres on the graphene oxide (Fig. 3b). The nano silver spheres are deposited on the reduced graphene oxide by PPy overlay as shown in Fig. 3c and 3d. As can be analyzed from FESEM pictures, the shape and size of AgNPs are globular and smaller than 75 nm.

3.4 XPS analysis

XPS was applied to investigate the chemical composition of PPy@Ag/rGO nanocomposite. The XPS spectra clearly reveal that the existence of N, C, O, Ag in PPy@Ag/rGO nanocomposite (Fig. 4a). Figure 4d shows the peaks present at a binding energy of 398.4 eV for neutral benzenoid amine nitrogen(-NH-), 398.9 eV for protonated benzenoid amine nitrogen (N^+), 396.5 eV for quinonoid imine nitrogen (-N=), and 405.7 eV for nitrate ion(NO_3^{-1}), rerespectively [45]. The C 1s can be deconvoluted into 283.3 eV, 284.5 eV and 285.9 eV assigned to C-C, C-N and = C-NH^+, respectively (Fig. 4c). In Fig. 4d, XPS spectra shows the peak of Ag and a doublet peak of Ag (3d) arising from spin-orbit coupling (Ag $3d_{5/2}$ at 366.5 eV and Ag $3d_{3/2}$ at 372.5 eV).

3.5 Antibacterial Activities

The antibacterial activities of these prepared nanocomposites were evaluated by bacterium colony computation in the experiment (Fig. 5). The medium without antibacterial material was regarded as a blank control sample (Fig. 5a). For blank control sample, *E. coli* bacteria show very good in stark contrast to the experimental groups. In the experimental groups with nanomaterials, fewer *E. coli* colonies (Fig. 5b-d) grow on medium, showing superior antibacterial activity against *E. coli* colonies. Among them, PPy@Ag/rGO nanomaterials exhibited the best antibacterial properties, killing almost 99% of *E. coli*.

In order to study the changes of bacterial morphology with nanocomposites during the bacteriostatic process, the *E.coli* affected by PPy@Ag/rGO nanocomposites was observed by TEM, as shown in Fig. 6. It is found that large amounts of nanocomposites are distributed around the membrane of bacteria during sterilization and tend to enter the interior of the cell. In addition, the bacterial morphology of *E. coli* has undergone significant changes. The smooth and clear cell membrane of *E. coli* became rough and wrinkled, indicating that the bacterial cell membrane has been destroyed and lost its original barrier function.

Figure 7 shows the experimental results of liquid antibacterial. The liquid antibacterial effect of different antibacterial materials is seen in Fig. 7a. The Ag/rGO and PPy@Ag/rGO nanocomposites exhibit high antibacterial activity. To explore the effect of PPy on antimicrobial activity, we performed a cycling experiment on antimicrobial materials. From the analysis in Fig. 7b, Ag/rGO and PPy@Ag/rGO nanocomposites show higher antibacterial activity when they are initially used. However, as the number of cycles increases, the antibacterial activity of Ag/rGO nanomaterials significantly decreases due to the loss of nanosilver. PPy has a stabilizing effect on nano-silver in PPy@Ag/rGO nanocomposites, which can reduce the loss of nano-silver and thus maintain high antibacterial activity for a long time (Fig. 7c).

Table 1

Time lapse record of metal ions concentrations such as Ag^+ ion released from Ag/rGO and PPy@Ag/rGO nanocomposite after immersion in LB medium (0.2 mg/mL) determined by inductively coupled plasma (ICP)

Sample	Ag^+ ion in LB medium(mmol/L)					
	0h	3h	6h	9h	12h	24h
Ag/rGO	0	0.0447	0.0987	0.1105	0.1278	0.1400
PPy@Ag/rGO	0	0.0017	0.003	0.0039	0.0048	0.0069

In order to study the antibacterial mechanism of the nanocomposite PPy@Ag/rGO. We first used ICP to detect the concentration of silver ions immersed in LB medium during liquid antibacterial processes. As a result, as shown in Table 1, the leakage of silver ions is small. This indicates that the nanocomposite does not inhibit and kill bacteria by leakage of precious metals. In addition, we also performed zeta potential testing on nanocomposites. The experimental results show that the polymer PPy and the nanocomposite PPy@Ag/rGO are positively charged in physiological saline (Fig. 8). At the same time, we performed electron paramagnetic resonance analysis on nanocomposites. The results show that nanomaterials do not produce hydroxyl radicals and superoxide radicals under dark conditions (Fig. 11). Based on the comprehensive test and TEM results analysis, we propose a possible antibacterial mechanism. Polypyrrole in nanocomposites exhibits a positive affinity for electronegative *E. coli* due to its electropositive properties. Therefore, *E. coli* will accumulate on polypyrrole. The nano-silver particles dispersed on polypyrrole and reduced graphene oxide cause the bacteria to die by reducing the integrity of the bacterial membrane and rupturing the *E. coli* cell membrane.

3.6 Photocatalytic performances

The photocatalytic activity of the nanocomposite was evaluated under visible light by photocatalytic degradation of TC. In this way, the application prospect of composite photocatalyst in environmental water treatment was evaluated (Fig. 9a). The adsorption-desorption balance between the degraded liquid and the sample is achieved prior to the start of the reaction. In these experiments, the photodegradation efficiency of TC on the PPy/rGO nanocomposite is only 37.91%, while the TC removal ratios of Ag/rGO and PPy@Ag/rGO are 73.72% and 80.88%, respectively, which is attributed to the surface plasmon resonance effect of nano-silver. Through the analysis of the results of the cycle experiment, the addition of polymer PPy helps to increase the photocatalytic stabilizing ability of nanomaterials (Fig. 9b).

The transient photocurrent response (Fig. 10a) is used to manifest the exciton separation rates of the as-prepared samples [46]. The photocurrent intensity is significantly enhanced from PPy/rGO to PPy@Ag/rGO, which verifies the most efficient separation of excitons in PPy@Ag/rGO. Electrochemical impedance spectra (EIS) (Fig. 10b) are also collected to disclose the charge carriers transfer resistance of the as-prepared samples. It is well-known that the smaller radius of EIS plot suggests the lower resistance in charge transport or, in other words, the higher charge transfer rate on the interfaces [47]. PPy@Ag/rGO

shows the highest the transport ability of photoinduced charge carriers from inside to surface, consistent with the photocurrent result.

In order to understand the active substances generated during photocatalysis and the mechanism of degradation, the DMPO spin-trapping ESR technique is employed. As seen in Fig. 11, a significant characteristic peak of DMPO-•O_2^- appears of the PPy@Ag/rGO sample under visible light irradiation. In contrast, no peaks were produced under dark conditions. Similarly, the four characteristic peaks of DMPO-•OH also only show under visible light. Secondly, the active substance capture experiment was carried out to determine the main active substances in the photocatalytic procedure. The superoxide radicals (•O_2^-), holes (h^+) and hydroxyl radicals (•OH) were captured by the addition of the capture scavenger ascorbic acid (VC), triethanolamine (IPA) and isopropanol (TEOA), respectively. The results are shown in Fig. 12, indicating that the three actives •O_2^-, h^+ and •OH play an important role in the photodegradation of TC.

4. Conclusion

In a word, an environmentally friendly, simple and easy method was developed to synthesize PPy@Ag/rGO nanocomposites. Ag NPs with a monodisperse size are well dispersed on the surface of the PPy/rGO nano-flakes. In addition, PPy is Ag NPs as stabilizers to prevent loss. At the same time, PPy has a strong affinity for *E. coli*. PPy@Ag/rGO Nano-complexes show very low cytotoxicity and highly effective antimicrobial activity against *E. coli*. The antibacterial activity of PPy@Ag/rGO nanocomposites against *E. coli* can reach 98%, and have long-term effective antibacterial activity. The PPy@Ag/rGO nanocomposites also have a good degradation effect on the antibiotic tetracycline. In summary, PPy@Ag/rGO is a promising nanocomposite for the removal of antibiotics and bacteria in the environment.

Declarations

Acknowledgements

This work was supported by Zhangjiagang Science and Technology Support Program (Social Development) of Jiangsu Province, China (grant number:ZKS1510).

References

[1] V.H. Nguyen, B.K. Kim, Y.L. Jo, J.J. Shim, Preparation and antibacterial activity of silver nanoparticles-decorated graphene composites, J. Supercrit. Fluids **72**, 28-35 (2012)

[2] W. Teng, X.J. Tan, X.Y. Li, Y.B. Tang, Novel Ag_3PO_4/MoO_3 p-n heterojunction with enhanced photocatalytic activity and stability under visible light irradiation, Appl. Surf. Sci. **409**, 250-260 (2017)

[3] P. Madhavan, P.Y. Hong, R. Sougrat, S.P. Nunes, Silver-enhanced block copolymer membranes with biocidal activity, ACS Appl. Mater. Interfaces **6**, 18497-18501 (2014)

[4] M.R. Bindhu, M. Umadevi, Antibacterial and catalytic activities of green synthesized silver nanoparticles, Spectroc. Acta Pt. A-Molec. Biomolec. Spectr. **135**, 373-378 (2015)

[5] Y. Wen, H. Ding, Y. Shan, Preparation and visible light photocatalytic activity of Ag/TiO_2/graphene nanocomposite, Nanoscale **3**, 4411-4417 (2011)

[6] J. Low, J. Yu, Q. Li, Enhanced visible-light photocatalytic activity of plasmonic Ag and graphene co-modified Bi_2WO_6 nanosheets, Phys. Chem. Chem. Phys. **16**, 1111-1120 (2014)

[7] W.F. Li, R. Yu, M. Li, N. Guo, H.W. Yu, Y. Yu, Photocatalytical degradation of diclofenac by Ag-BiOI-rGO: Kinetics, mechanisms and Pathways, Chemosphere **218**, 966-973 (2019)

[8] F.P. Cai, Y.B. Tang, F.Y. Chen, Y. Yan, W.D. Shi, Enhanced visible-light-driven photocatalytic degradation of tetracycline by Cr^{3+} doping $SrTiO_3$ cubic nanoparticles, RSC Adv. **5**, 21290-21296 (2015)

[9] W. Yu, Z. Xiao, X. Li, S. Song, L. Chen, J. Shen, Dry plasma synthesis of graphene oxide-Ag nanocomposites: A simple and green approach, Mater. Res. Bull. **53**, 145-150 (2014)

[10] Y. Li, Y. Cao, J. Xie, D. Jia, H. Qin, Z. Liang, Facile solid-state synthesis of Ag/graphene oxide nanocomposites as highly active and stable catalyst for the reduction of 4-nitrophenol, Catal. Commun. **58**, 21-25 (2015)

[11] J. Xu, B.F. Luo, W. Gu, Y.P. Jian, F.L. Wu, Y.B. Tang, H. Shen, Fabrication of In_2S_3/$NaTaO_3$ composites for enhancing the photocatalytic activity toward the degradation of tetracycline, New J. Chem. **42**, 5052-5058 (2018)

[12] T. Ali, A. Ahmed, U. Alam, Enhanced photocatalytic and antibacterial activities of Ag-doped TiO_2 nanoparticles under visible light, Mater. Chem. Phys. **212**, 325-335 (2018)

[13] Q. Liu, E. Liu, J. Li, Y. Qiu, R. Chen, Rapid ultrasonic-microwave assisted synthesis of spindle-like Ag/ZnO nanostructures and their enhanced visible-light photocatalytic and antibacterial activities, Catal. Today (2019)

[14] X. Wang, P. Huang, L. Feng, M. He, S. Guo, G. Shen, Green controllable synthesis of silver nanomaterials on graphene oxide sheets via spontaneous reduction, RSC Adv. **2**, 3816-3822 (2012)

[15] H. Wang, C.F. Yang, M. Li, F.Y. Chen, Y.J. Cui, Enhanced photocatalytic hydrogen production of restructured B/F codoped g-C_3N_4 via post-thermal treatment, Mater. Lett. **212**, 319-322 (2018)

[16] Y.J. Cui, M. Li, H. Wang , C.F. Yang, S.G. Meng, F.Y. Chen, In-situ synthesis of sulfur doped carbon nitride microsphere for outstanding visible light photocatalytic Cr(VI) reduction, Sep. Purif. Technol. **199**,

251-259 (2018)

[17] W. Hu, C. Peng, W. Luo, M. Lv, X. Li, D. Li, Graphene-based antibacterial paper, Acs Nano **4**, 4317-4323 (2010)

[18] J. Chen, H. Peng, X. Wang, F. Shao, Z. Yuan, H. Han, Graphene oxide exhibits broad-spectrum antimicrobial activity against bacterial phytopathogens and fungal conidia by intertwining and membrane perturbation, Nanoscale **6**, 1879-1889 (2014)

[19] S. Liu, T.H. Zeng, M. Hofmann, E. Burcombe, J. Wei, R. Jiang, Antibacterial activity of graphite, graphite oxide, graphene oxide, and reduced graphene oxide: membrane and oxidative stress, Acs Nano **5**, 6971-6980 (2011)

[20] O. Akhavan, E. Ghaderi, Photocatalytic Reduction of Graphene Oxide Nanosheets on TiO_2 Thin Film for Photoinactivation of Bacteria in Solar Light Irradiation, J. Phys. Chem. C **113**, 20214-20220 (2009)

[21] S. Liu, M. Hu, T.H. Zeng, R. Wu, R. Jiang, J. Wei, Lateral dimension-dependent antibacterial activity of graphene oxide sheets, Langmuir **28**, 12364-12372 (2012)

[22] Z. Wang, D. Tonderys, S.E. Leggett, E.K. Williams, M.T. Kiani, R.S. Steinberg, Wrinkled, wavelength-tunable graphene-based surface topographies for directing cell alignment and morphology, Carbon **97**, 14-24 (2016)

[23] Y. Han, Z. Luo, L. Yuwen, J. Tian, X. Zhu, L. Wang, Synthesis of silver nanoparticles on reduced graphene oxide under microwave irradiation with starch as an ideal reductant and stabilizer, Appl. Surf. Sci. **266**, 188-193 (2013)

[24] M.Y. Li, Y.B. Tang, W.L. Shi, F.Y. Chen, Y. Shi, H.C. Gu, Design of visible-light-response core-shell $Fe_2O_3/CuBi_2O_4$ heterojunctions with enhanced photocatalytic activity towards the degradation of tetracycline: Z-scheme photocatalytic mechanism insight, Inorg. Chem. Front. **5**, 3148-3154 (2018)

[25] P.W. Huo, C.Y. Liu, D.Y. Wu, Fabricated Ag/Ag_2S/reduced graphene oxide composite photocatalysts for enhancing visible light photocatalytic and antibacterial activity, J. Ind. Eng. Chem. **57**, 125-133 (2017)

[26] E.R. Kenawy, S.D. Worley, R. Broughton, The Chemistry and Applications of Antimicrobial Polymers: A State-of-the-Art Review. Biomacromolecules **8**, 1359-1384 (2007)

[27] G.N. Tew, R.W. Scott, M.L. Klein, W.F. Degrado, De Novo Design of Antimicrobial Polymers, Foldamers, and Small Molecules: From Discovery to Practical Applications, Accounts Chem. Res. **43**, 30-39 (2010)

[28] L. Timofeeva, N. Kleshcheva, Antimicrobial polymers: mechanism of action, factors of activity, and applications, Appl. Microbiol. Biotechnol. **89**, 475-492 (2011)

[29] A. Varesano, C. Vineis, A. Aluigi, F. Rombaldoni, C. Tonetti, G. Mazzuchetti, Antibacterial efficacy of polypyrrole in textile applications, Fiber. Polym. **14**, 36-42 (2013)

[30] J.H. Chen, J.K. Xu, K. Wang, X. Qian, R.C. Sun, Highly Thermostable, Flexible and Conductive Films Prepared from Cellulose, Graphite and Polypyrrole Nanoparticles, ACS Appl. Mater. Interfaces **7**, 15641-15648 (2015)

[31] W. Sun, L. Chen, Y. Wang, Synthesis of Highly Conductive PPy/Graphene/MnO_2 Composite Using Ultrasonic Irradiation, Synth. Rect. Inorg. Metal **46**, 437-444 (2016)

[32] G. Catalanotti, A. Katunin, Modelling the electro-mechanical properties of PPy/epoxy conductive composites, Comp. Mater. Sci. **113**, 88-97 (2016)

[33] T.J. Pan, X.W. Zuo, T. Wang, Electrodeposited conductive polypyrrole/polyaniline composite film for the corrosion protection of copper bipolar plates in proton exchange membrane fuel cells, J. Power Sources 302, 180-188 (2016)

[34] F. Zhao, L. Liu, F. Yang, E-Fenton degradation of MB during filtration with Gr/PPy modified membrane cathode, Chem. Eng. J. **230**, 491-498 (2013)

[35] Y.C. Jia, P. Xiao, H.C. He, J.Y. Yao, F.L. Liu, Photoelectrochemical properties of polypyrrole/TiO_2 nanotube arrays nanocomposite under visible light, Appl. Surf. Sci. **258**, 6627-6631 (2012)

[36] J. Joo, J.K. Lee, S.Y. Lee, K.S. Jang, E.J. Oh, A.J. Epstein, Physical Characterization of Electrochemically and Chemically Synthesized Polypyrroles, Macromolecules **33**, 5131-5136 (2000)

[37] C. Wan, J. Li, Cellulose aerogels functionalized with polypyrrole and silver nanoparticles: In-situ synthesis, characterization and antibacterial activity, Carbohydr. Polym. **146**, 362-367 (2016)

[38] W.S.H. Jr, R.E. Offeman, Preparation of Graphitic Oxide, J. Am. Chem. Soc. **80**, 1339 (1958)

[39] O. Akhavan, E. Ghaderi, Toxicity of graphene and graphene oxide nanowalls against bacteria, Acs Nano **4**, 5731-5736 (2010)

[40] Y. Cheng, X. Zhao, X. Liu, W. Sun, H. Ren, G. Bo, Antibacterial activity and biological performance of a novel antibacterial coating containing a halogenated furanone compound loaded poly(L-lactic acid) nanoparticles on microarc-oxidized titanium, Int. J. Nanomed. **10**, 727-737 (2015).

[41] B.S. Singu, K.R. Yoon, Synthesis and characterization of MnO_2-decorated graphene for supercapacitors, Electrochim. Acta **231**, 749-758 (2017)

[42] C. Zhao, K. Shu, C. Wang, S. Gambhir, G.G. Wallace, Reduced graphene oxide and polypyrrole/reduced graphene oxide composite coated stretchable fabric electrodes for supercapacitor application, Electrochim. Acta **172**, 12-19 (2015)

[43] A. Singh, Z. Salmi, N. Joshi, P. Jha, P. Decorse, H. Lecoq, Electrochemical investigation of free-standing polypyrrole-silver nanocomposite films: a substrate free electrode material for supercapacitors, RSC Adv. **3**, 24567 (2013)

[44] P. Dallas, D. Niarchos, D. Vrbanic, N. Boukos, S. Pejovnik, C. Trapalis, Interfacial polymerization of pyrrole and in situ synthesis of polypyrrole/silver nanocomposites, Polymer **48**, 2007-2013 (2007)

[45] J. Cao, Y. Wang, J. Chen, X. Li, F.C. Walsh, J.H. Ouyang, Three-dimensional graphene oxide/polypyrrole composite electrodes fabricated by one-step electrodeposition for high performance supercapacitors, J. Mater. Chem. A **3**, 14445-14457 (2015).

[46] L. Shi, T. Wang, H. Zhang, K. Chang, X. Meng, H. Liu, J. Ye, An Amine-Functionalized Iron(III) Metal-Organic Framework as Efficient Visible-Light Photocatalyst for Cr(VI) Reduction Adv. Sci. **2**, 1500006 (2015)

Figures

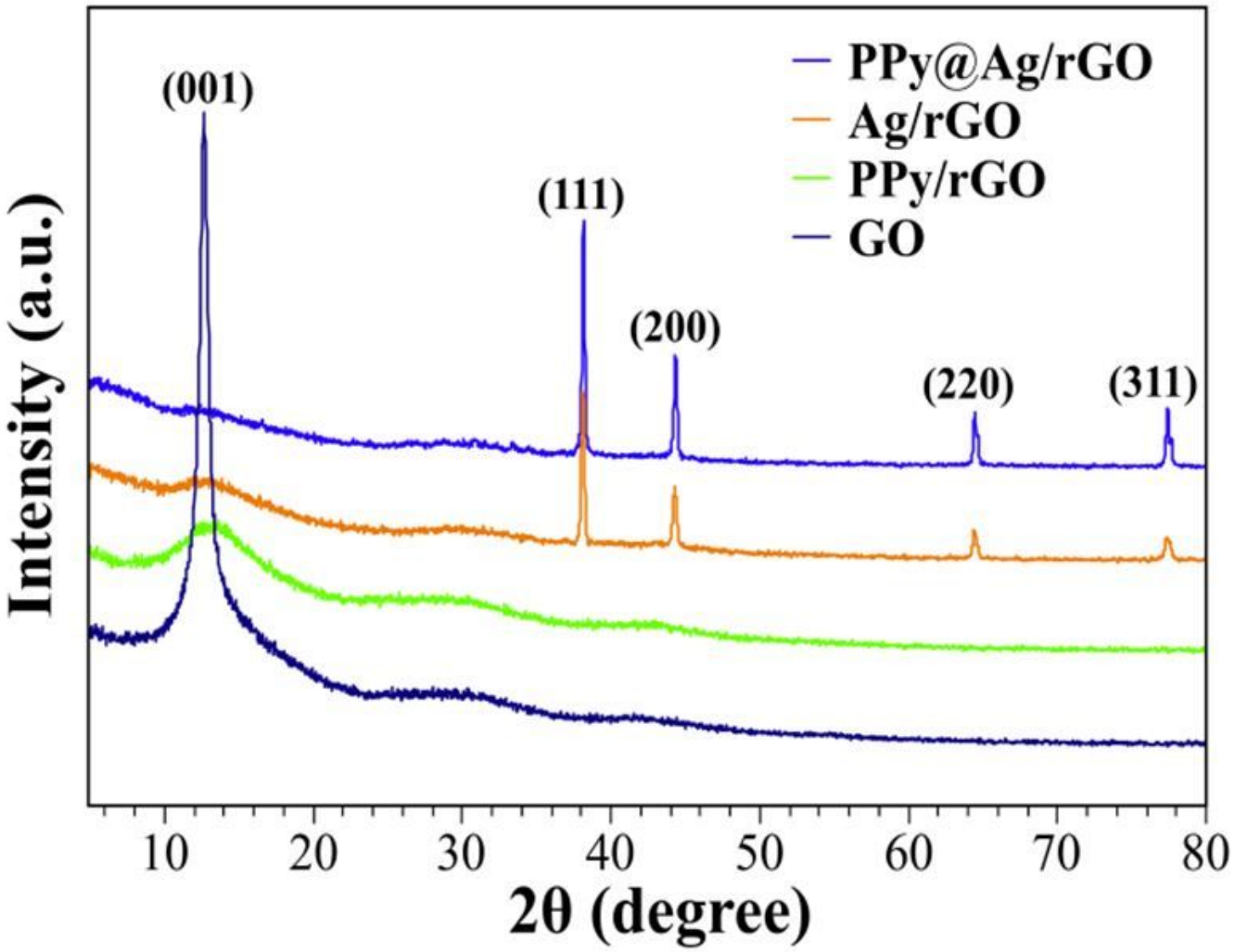

Figure 1

XRD patterns of PPy/rGO, Ag/rGO and PPy@Ag/rGO nanocomposites

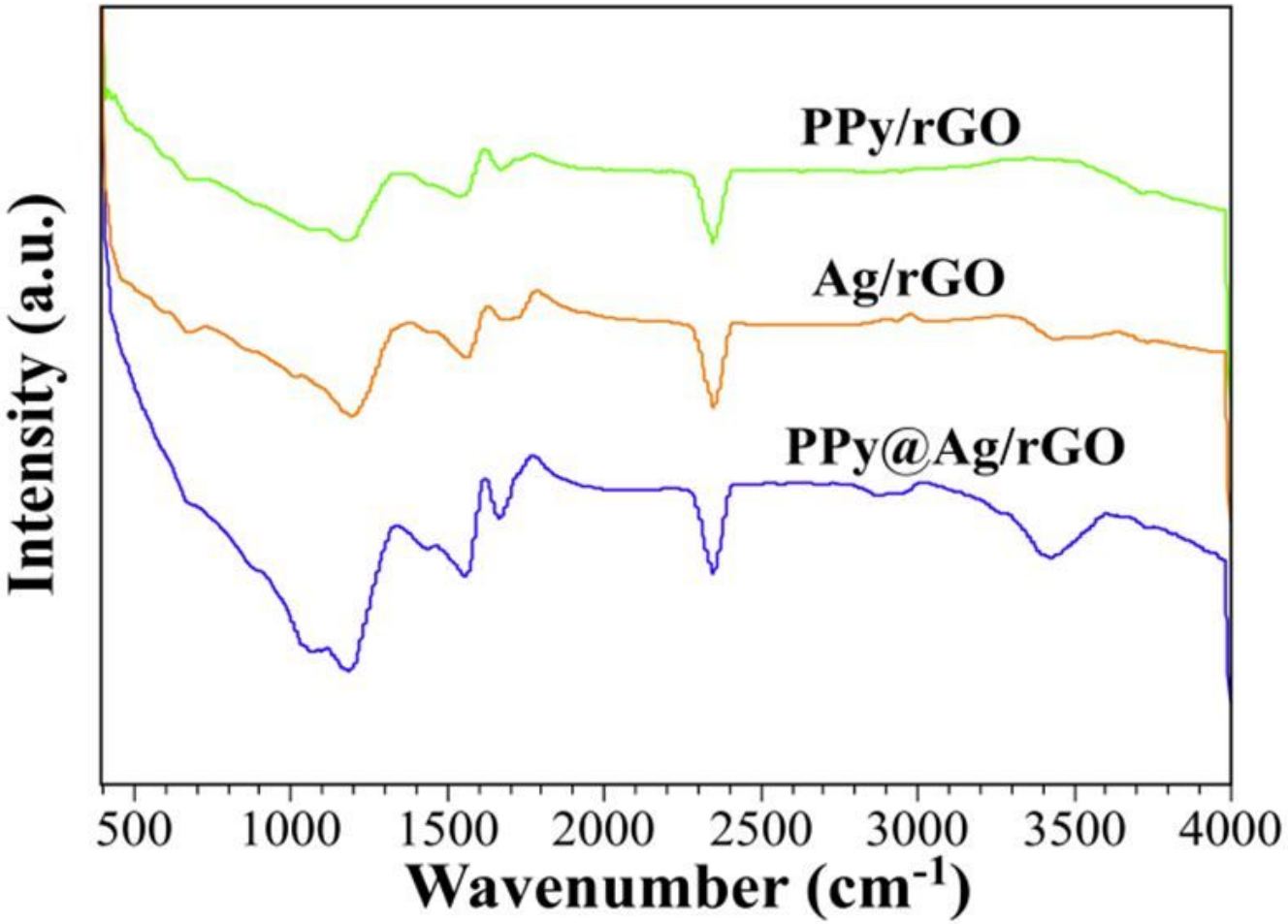

Figure 2

FT-IR spectra of PPy/rGO, Ag/rGO and PPy@Ag/rGO nanocomposites

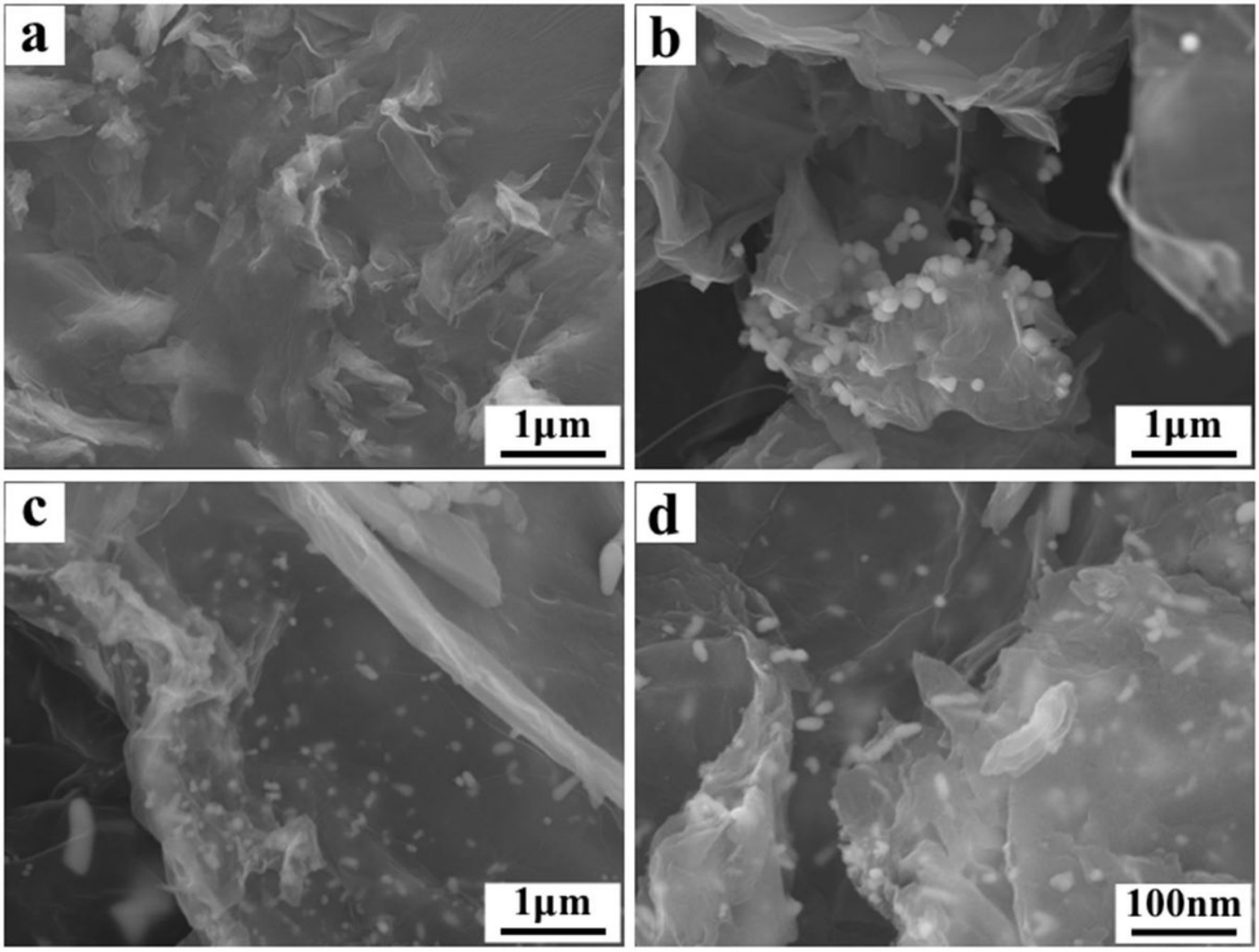

Figure 3

FE-SEM images of (a) PPy/rGO , (b) Ag/rGO, (c,d) PPy@Ag/rGO

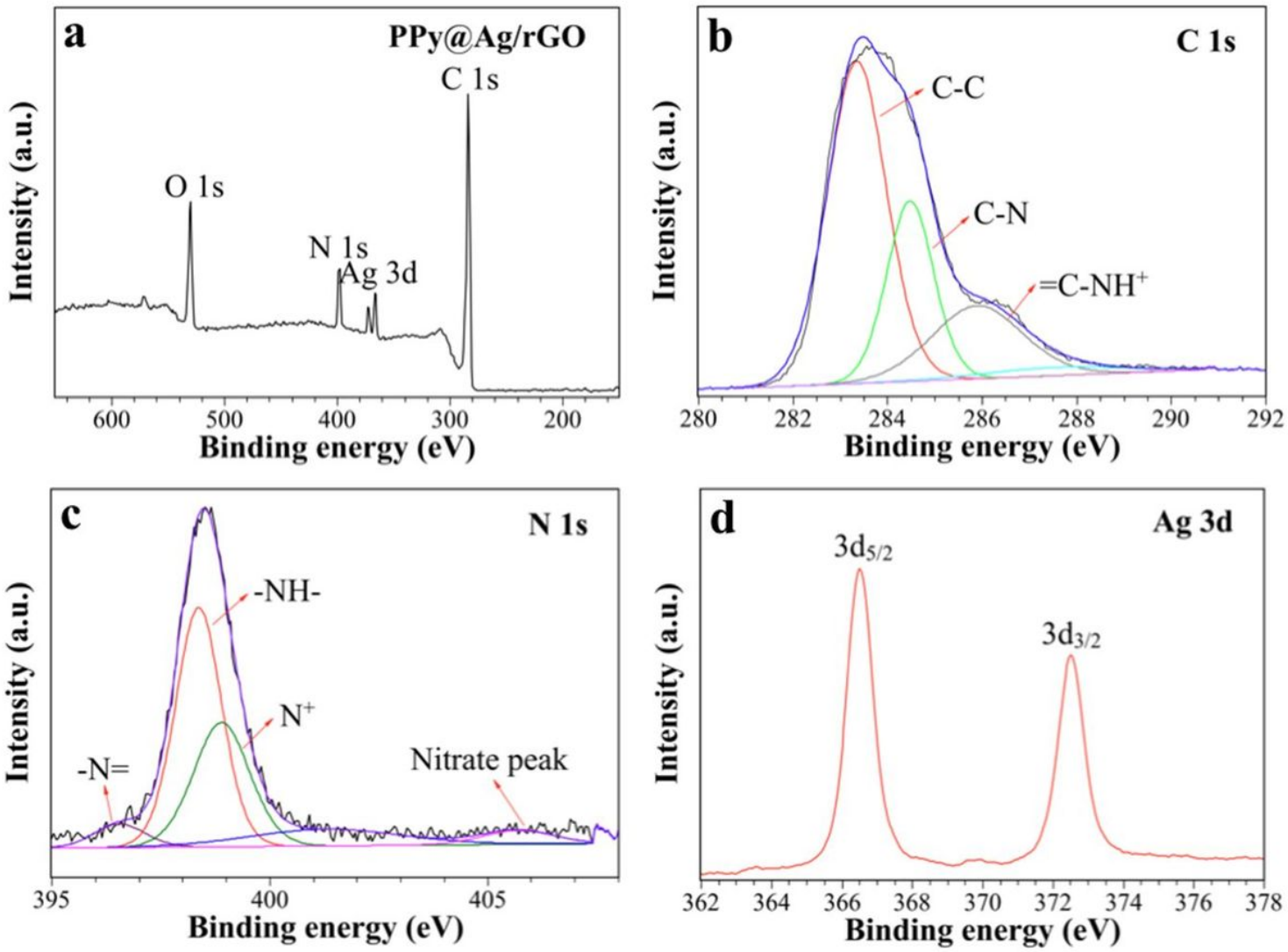

Figure 4

(a) XPS survey spectra for PPy@Ag/rGO composites, (b) high resolution C1s of PPy@Ag/rGO, (c) high resolution N1s of PPy@Ag/rGO ,and (d) Ag3d from PPy@Ag/rGO

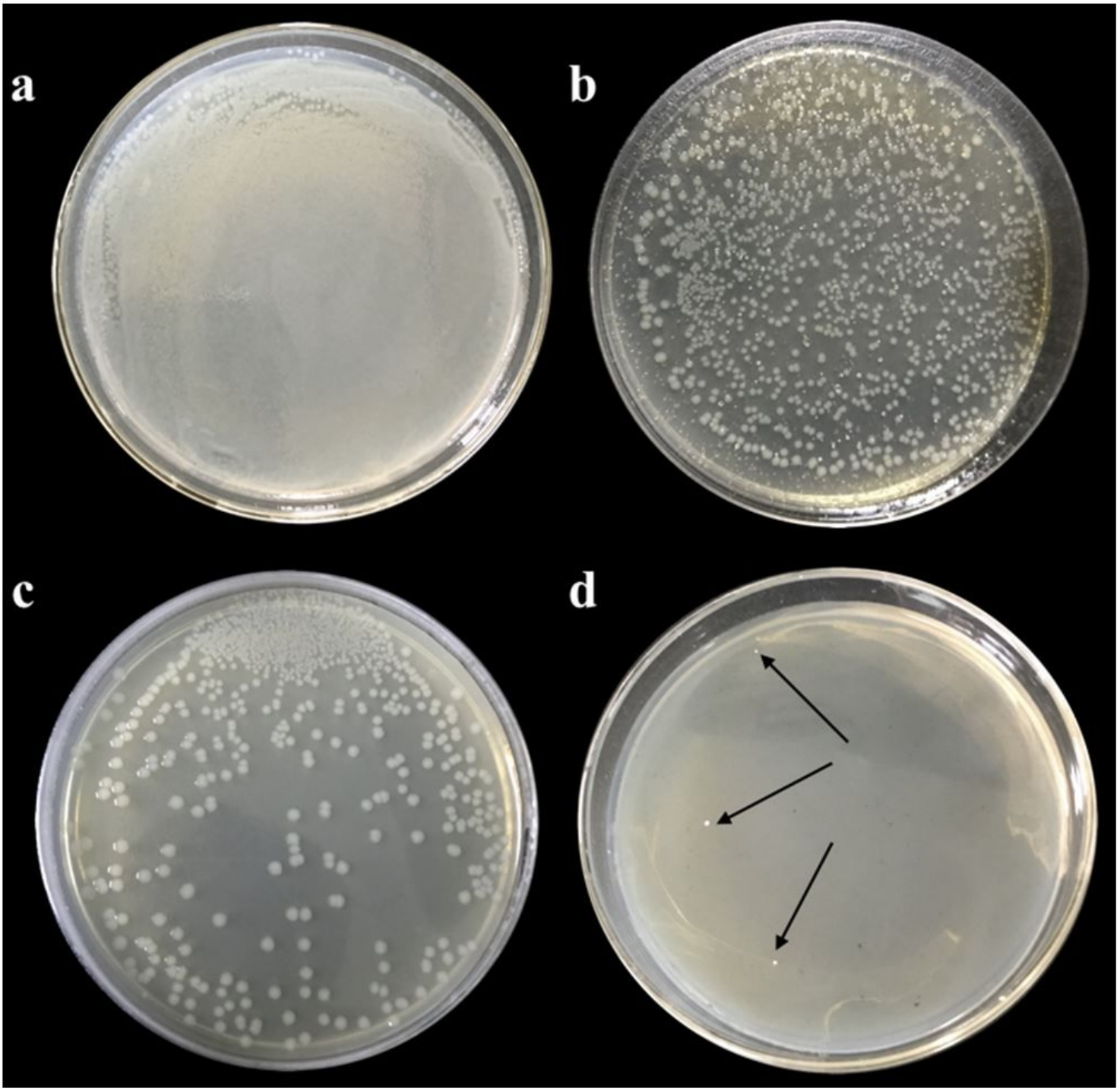

Figure 5

Digital image of colony-forming unit of E. coli incubated (a) on the control blank medium, (b) PPy/rGO, (c) Ag/rGO, (d) PPy@Ag/rGO

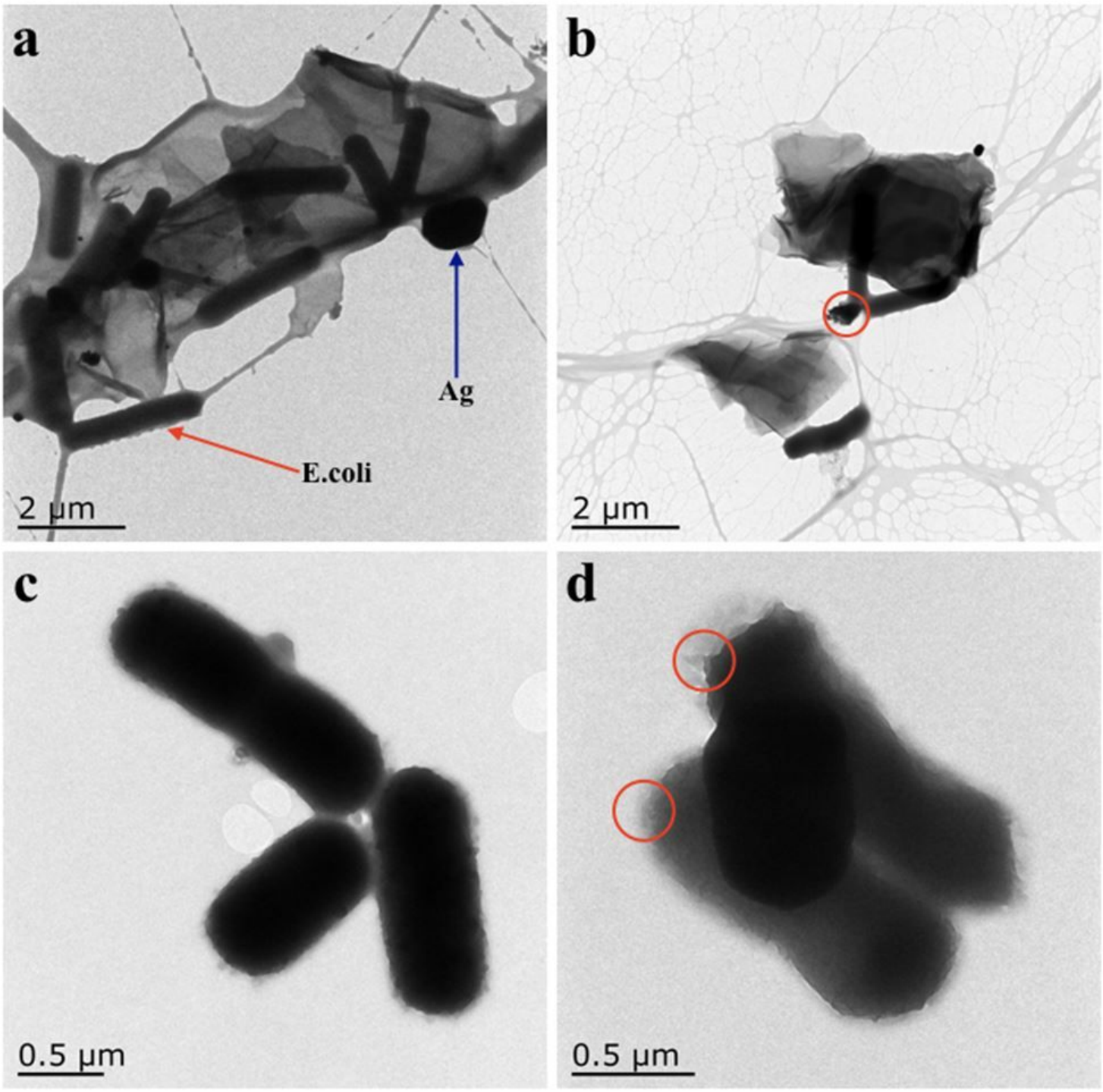

Figure 6

(a,b) TEM images of E. coli after treatment with PPy@Ag/rGO nanocomposites, (c) E.coli cells, (d) E.coli after treatment with 35 μg/mL PPy@Ag/rGO nanocomposites for 360 min

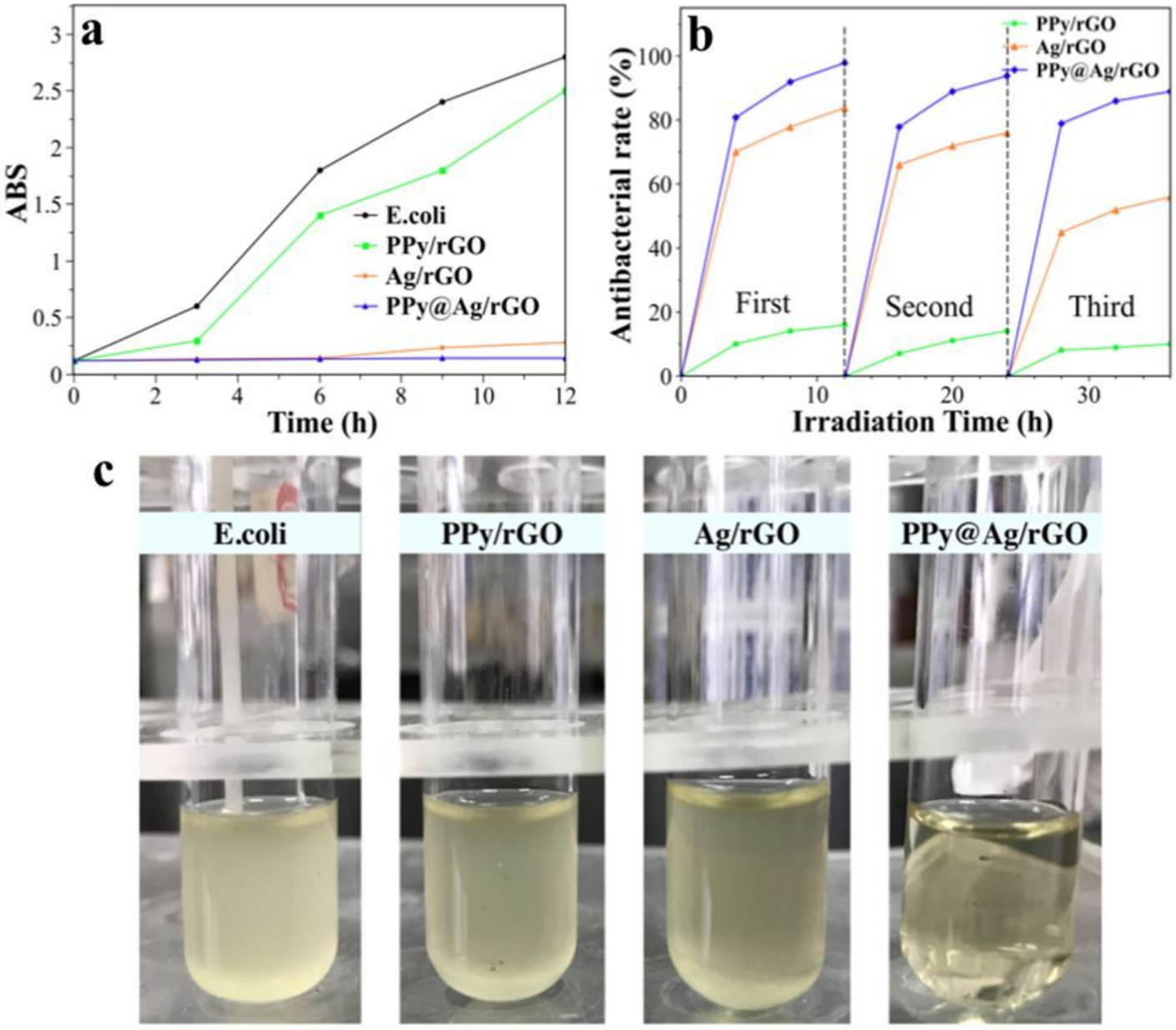

Figure 7

(a) The antibacterial rates of PPy/rGO,Ag/rGO and PPy@Ag/rGO in the natural condition the adsorption of different conditions, (b) Cycling runs for antibacterial activity of E. coli and (c) after three liquid antibacterial cycles runs of picture

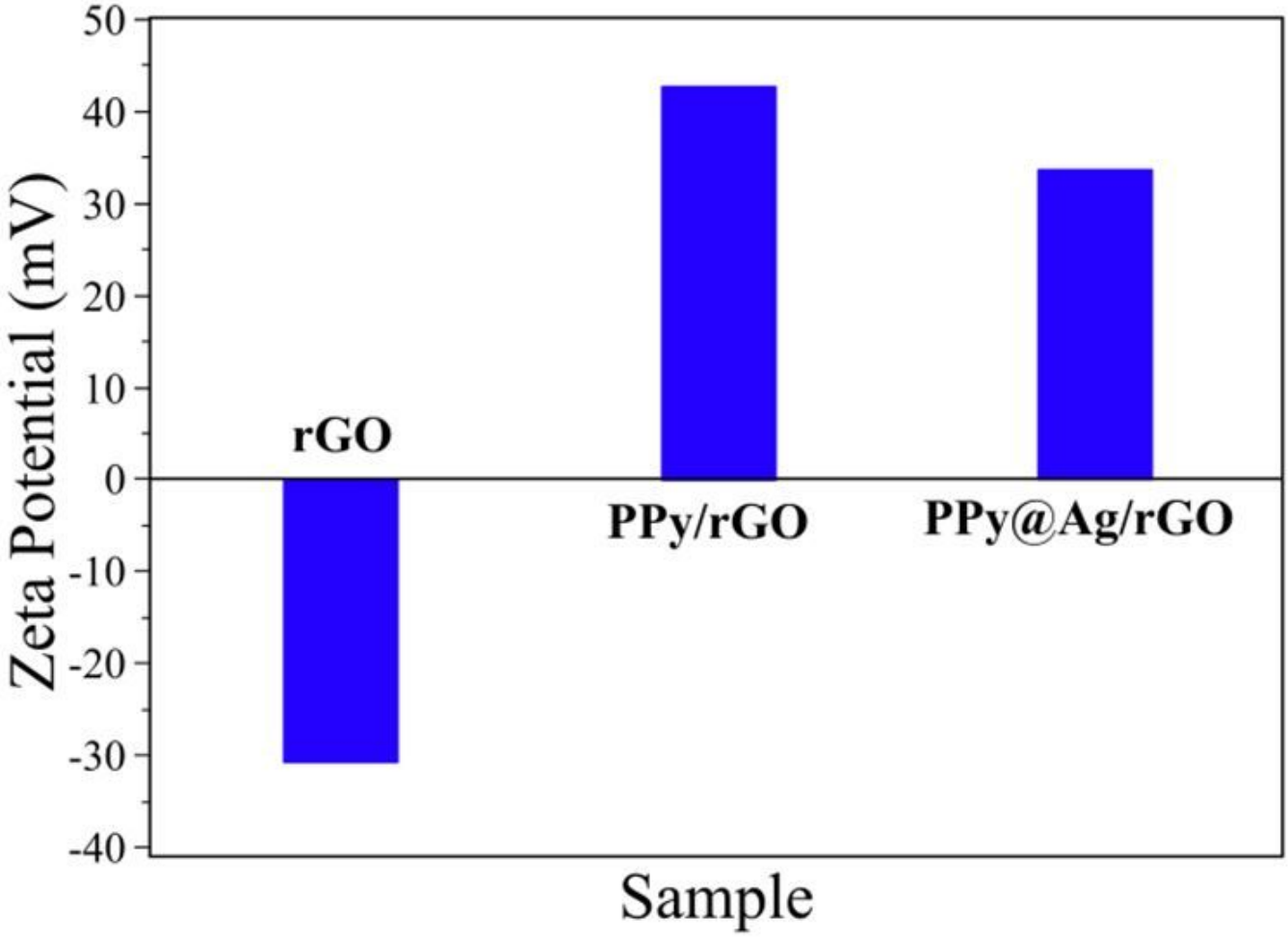

Figure 8

Zeta potential of rGO, PPy/rGO and PPy@Ag/rGO in saline, respectively

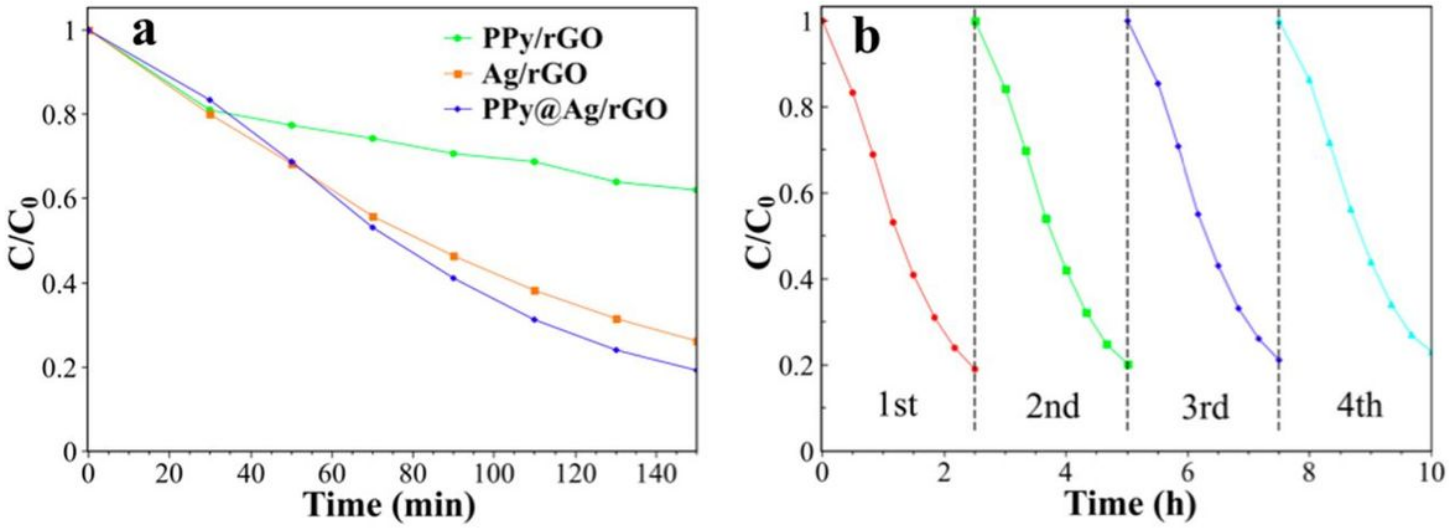

Figure 9

(a)Photocatalytic activities of PPy/rGO, Ag/rGO and PPy@Ag/rGO nanocomposites for TC under visible-light irradiation and (b) recycling photocatalytic degradation test of PPy@Ag/rGO

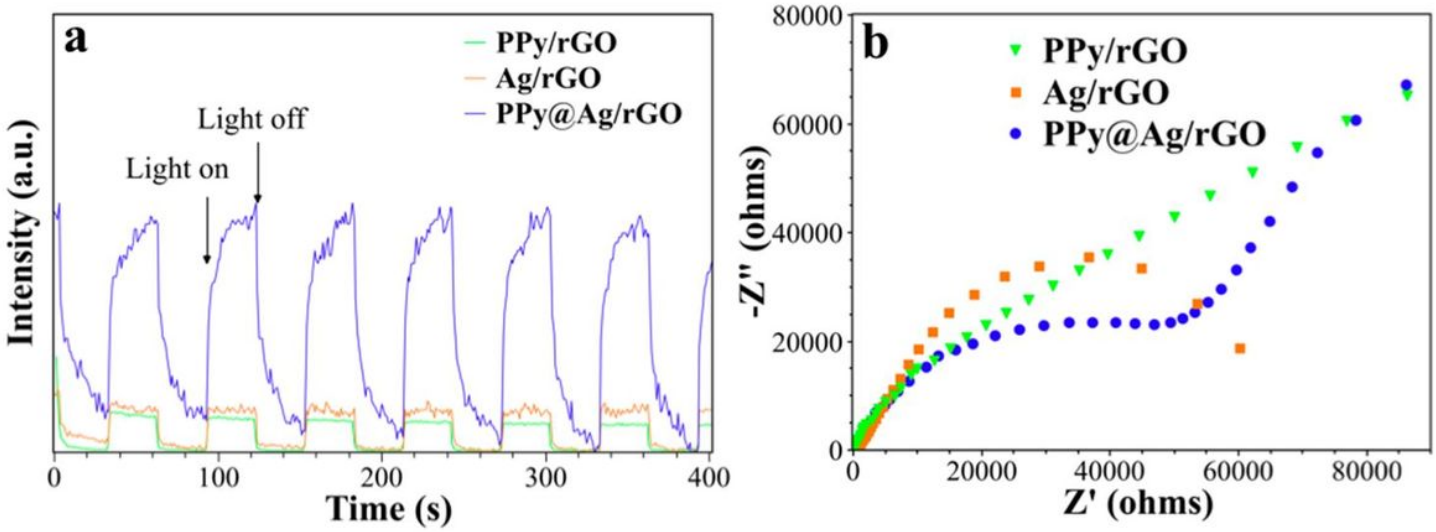

Figure 10

(a)Photocurrent transient response and (b) EIS Nyquist plots of samples

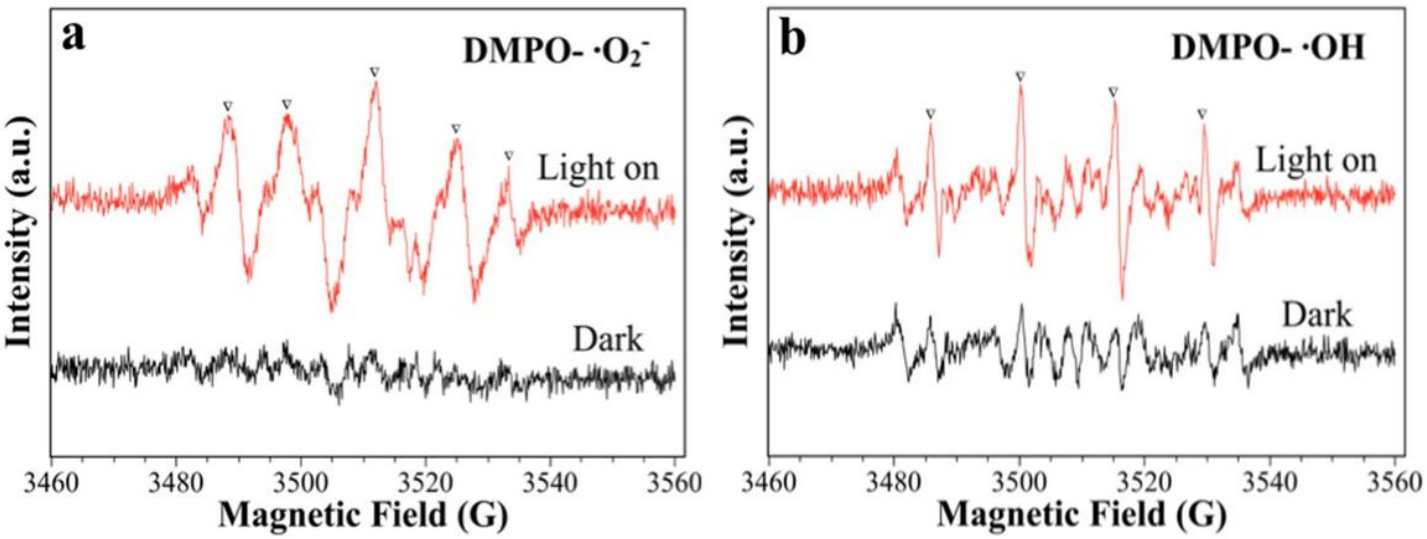

Figure 11

DMPO spin-trapping EPR spectra for (a) DMPO-•O2− over PPy@Ag/rGO in methanol dispersions and for (b) DMPO-•OH in aqueous dispersions

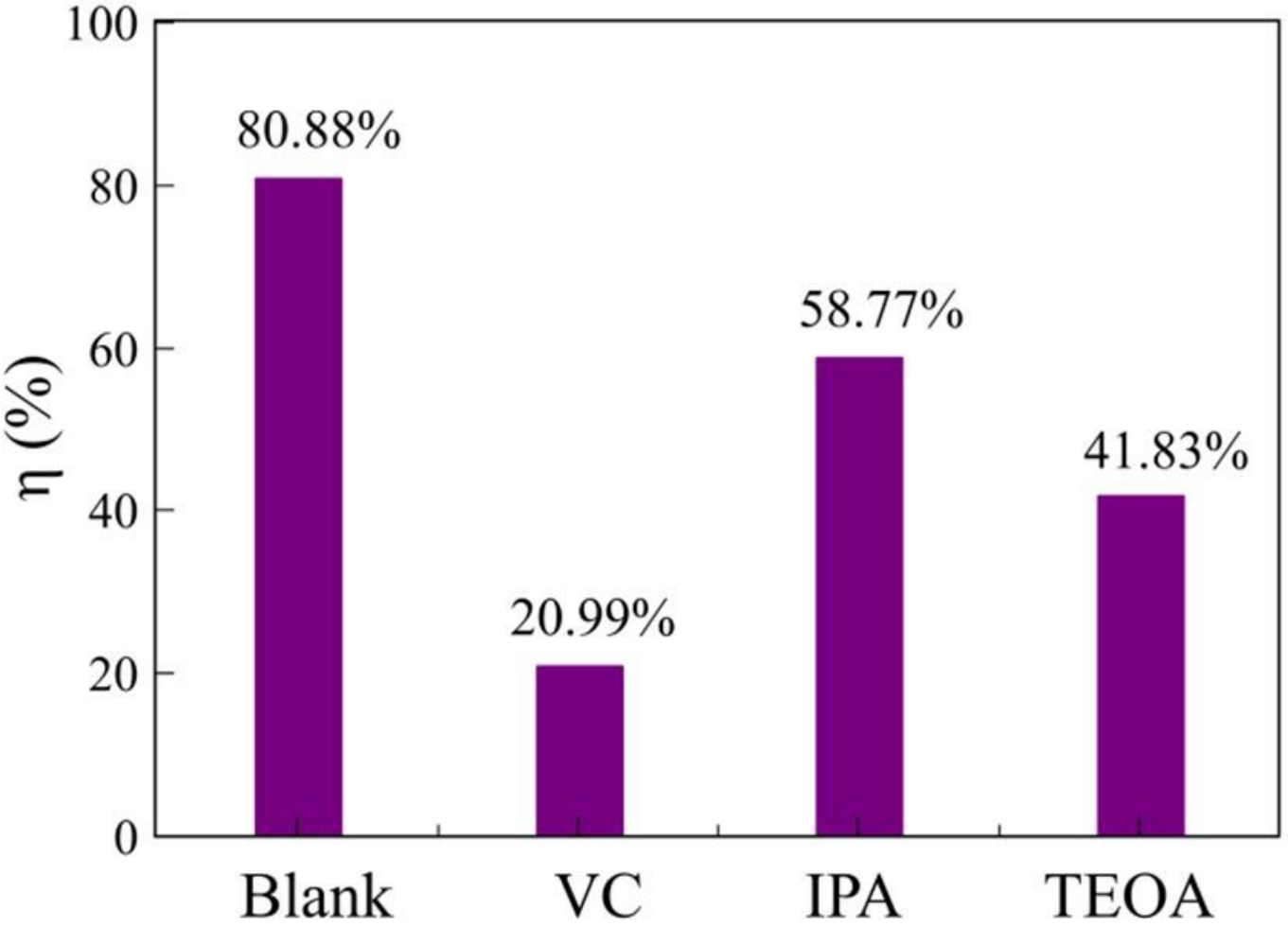

Figure 12

Reactive species trapping for the degradation of TC over the PPy@Ag/rGO under visible light irradiation

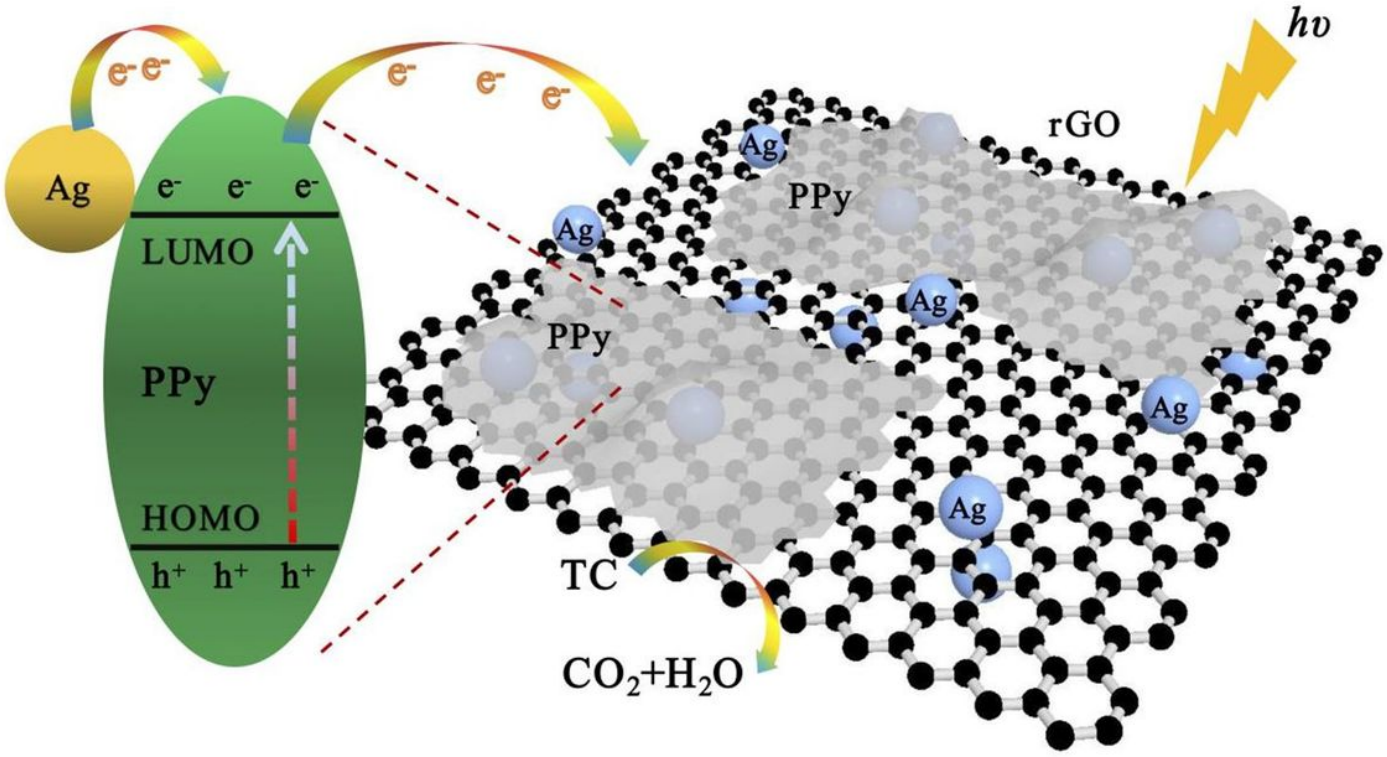

Figure 13

Schematic diagram of the reaction mechanism of photocatalytic degradation of TC.